

SAR DISTRIBUTION IN A BIO-MEDIUM IN CLOSE PROXIMITY WITH RECTANGULAR DIELECTRIC RESONATOR ANTENNA

R. K. Gangwar^{1, *}, **S. P. Singh**¹, and **D. Kumar**²

¹Department of Electronics Engineering, Institute of Technology, Banaras Hindu University, Varanasi 221005, India

²Department of Ceramic Engineering, Institute of Technology, Banaras Hindu University, Varanasi 221005, India

Abstract—In this paper, the simulation and experimental studies of SAR distribution in a bio-medium situated very close to a rectangular dielectric resonator antenna (RDRA) in C-band of microwave frequencies are reported. The simulation study has been carried out using CST Microwave Studio simulation software. The experimental distribution has been obtained using two 50 Ω L-shaped and straight probes and Agilent make 3 Hz–50 GHz spectrum analyzer. The experimental results for SAR distribution are compared with simulated results.

1. INTRODUCTION

The use of wireless portable devices is growing at fast rate throughout the world. These devices are often used in the vicinity of human body. The continuous growth of wireless portable devices has forced the worldwide researchers to study the interaction between the electromagnetic waves emanating from the device antenna and the human body. The human body, being lossy, absorbs certain amount of electromagnetic radiation generated from portable wireless device situated in its vicinity. This necessitates the evaluation of the performance of antenna in terms of input VSWR, return loss and bandwidth of antenna in presence of bio-medium on one hand and the estimation of the rate of electromagnetic energy absorption, known as specific absorption rate (SAR) in the body tissues on the other [1, 2]. The electric field induced and hence SAR within the human body

Received 13 April 2011, Accepted 1 June 2011, Scheduled 13 June 2011

* Corresponding author: Ravi Kumar Gangwar (ravi.gangwar.ece07@itbhu.ac.in).

depends on several factors including the strength and frequency of the external field, the shape, size and electrical characteristics of the body tissues and the orientation of the body in relation to the external field.

Dielectric Resonator Antennas (DRAs) are considered as one of the most suitable portable device antenna due to their low profile, high radiation efficiency, large bandwidth, flexible feed arrangement, wide range of material dielectric constants, ease of excitation, easily controlled characteristics and ease of integration with other active or passive microwave integrated circuit (MIC) components [3–7]. Only a few studies are reported in the literature on SAR distribution in bio-tissues due to DRAs radiating electromagnetic waves. The FDTD method has been applied for computing SAR distribution inside the human head and the effects of the human proximities including, the head, the hand, and the user's glasses on the antenna performance have been analyzed [8]. Off-center ring DRA has been designed and also used for evaluation of SAR distribution in human head [9]. The performance of rectangular DRA (RDRA) in close proximity with the user's body was studied with the help of a user's hand model [10].

This paper provides simulation and experimental investigations of SAR distribution in a homogenous phantom bio-medium (sucrose solution) in close proximity with rectangular DRA in C-band of microwave frequencies. The simulation study has been carried out using CST Microwave Studio simulation software and measurement of power (proportional to square of the magnitude of induced electric field)/SAR distribution has been performed with the help of Agilent make Spectrum analyzer at the antenna resonant frequency. The simulated results for SAR distribution are compared with experimental results.

2. ANTENNA GEOMETRY AND PHANTOM MUSCLE LAYER

The configuration of the rectangular DRA fabricated from $(\text{CaO} \cdot 4\text{ZnO} \cdot \text{Nb}_2\text{O}_5 \cdot \text{TiO}_2)$ ceramic material of dielectric constant $\epsilon_r = 15.19$, and loss tangent $\tan \delta = 0.0192$ is shown in Figure 1. A rectangular coordinate system with the Z -axis oriented along the axis of the RDRA and perpendicular to the ground plane, and the X - Y plane parallel to ground plane as well as top and bottom rectangular surfaces of RDRA has been considered. The DRA is placed on a conducting ground plane fabricated from copper conductor of size $60 \text{ mm} \times 60 \text{ mm} \times 4 \text{ mm}$. It is excited by a 50Ω coaxial probe of diameter equal to 1.3 mm , which was optimized to provide minimum return loss at the

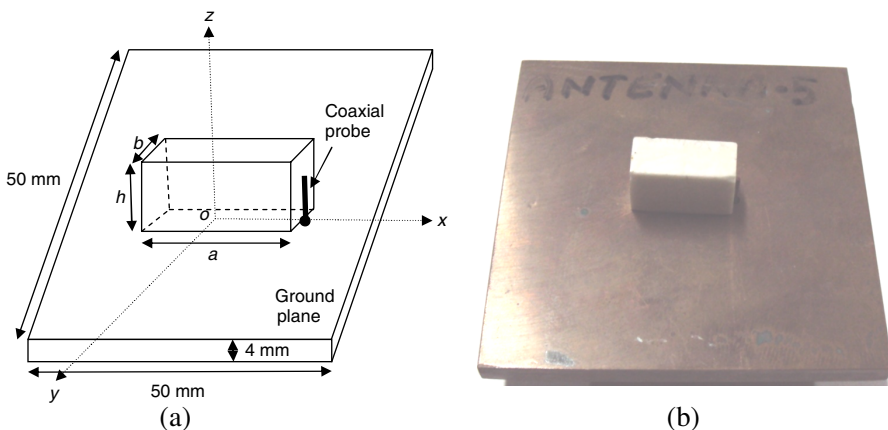


Figure 1. Antenna geometry. (a) Design layout. (b) Fabricated structure.

resonant frequency of antenna in free space. The DRA with dimensions $a = 19$ mm, $b = 8.2$ mm and height $h = 12$ mm was fabricated. The probe is located on the x -axis at $x = a/2$ and $\Phi = 0$.

For an RDRA of dimensions $a \times b \times h$, the resonant frequency for TE_{mnl}^y mode is calculated by solving the following equations [11, 12]:

$$k_y \tan\left(\frac{k_y b}{2}\right) = \sqrt{k_x^2 + k_z^2 - k_0^2} + \frac{1}{2}(n - 1)\pi$$

where $n = 1, 2, 3, \dots$ (1)

$$k_x^2 + k_z^2 + k_y^2 = k_0^2 \epsilon_r$$
 (2)

where k_0 denotes the free space wave number corresponding to the resonant frequency and k_x , k_y and k_z denote the wave numbers along the x , y and z -directions respectively. Wave numbers k_0 , k_x and k_z are determined by the following relation:

$$k_0 = \frac{2\pi}{\lambda_0} = \frac{2\pi f_o}{c}, \quad k_x = \frac{m\pi}{a}, \quad k_z = \frac{l\pi}{2h}$$

where λ_0 is the free space wavelength, f_o is the resonant frequency of the antenna in free space and c is the velocity of electromagnetic wave in free space.

For given resonator parameters ϵ_r , a , b , and h the resonant frequency of DRA is the one at which wave number k_y satisfies Equations (1) and (2). The resonant frequency f_o can be written as

$$f_o = \frac{c}{2\pi\sqrt{\epsilon_r}} \sqrt{k_x^2 + k_y^2 + k_z^2}$$
 (3)

Radiation Q -factor of RDRA can be written as [11]

$$Q = \frac{2\omega_0 W_e}{P_{rad}} \quad (4)$$

where W_e and P_{rad} are respectively the stored energy and radiated power of the RDRA and $\omega_0 (= 2\pi f_o)$ is the resonant angular frequency of the antenna in free space. The stored energy W_e and radiated power are given by

$$W_e = \frac{\varepsilon_r \varepsilon_0 a b h A^2}{32} \left(1 + \frac{\sin(k_y b)}{k_y b} \right) (k_x^2 + k_z^2)$$

and

$$P_{rad} = 10k_0^4 |p_m|^2$$

where, p_m is the magnetic dipole moment of the RDRA given by

$$p_m = \frac{-j8\omega\varepsilon_0(\varepsilon_r - 1)A}{k_x k_y k_z} \sin\left(\frac{k_y b}{2}\right)$$

and A is an arbitrary constant related to the maximum amplitude of the field.

The percentage bandwidth of RDRA is given by [11]

$$\%BW = \frac{S - 1}{Q\sqrt{S}} \times 100 \quad (5)$$

where S is the VSWR of RDRA.

The resonant frequency, Q -factor and bandwidth of the RDRA in free space for $TE_{2\delta 1}^y$ computed using Equations (3), (4) and (5) are found to be 5.227 GHz, 9.554 and 7.405% respectively.

The phantom muscle was prepared from the material composition given in reference [13], i.e., an aqueous solution of sucrose ($C_{12}H_{22}O_{11}$, 1.0 mol/l). The phantom muscle medium is prepared by mixing double distilled water with highly pure laboratory grade sucrose powder (obtained from Qualigens Fine Chemicals Pvt. Ltd, India). The real part of relative permittivity of the artificial muscle-model is assumed to be 50.95 at 5.25 GHz [13]. The electric conductivity of the muscle is assumed to 4.3231 S/m at 5.25 GHz. The phantom muscle was contained in one part of a chamber of inner dimensions 15 cm \times 15 cm \times 15 cm fabricated using perspex sheet of thickness equal to 4 mm. The perspex chamber shown in Figure 6 has been divided into two parts. One part (15 cm \times 15 cm \times 15 cm) contains the sucrose solution and is separated from the other part (15 cm \times 15 cm \times 5 cm) housing the antenna by miler sheet ($\varepsilon_r = 3.2$) of thickness 0.2 mm.

3. SIMULATION OF RDRA INPUT CHARACTERISTICS AND SAR DISTRIBUTION IN PHANTOM MUSCLE

The theoretical analysis involved in the design of some antennas can become quite complex and in many cases an exact solution may not be possible. Advances in computational electromagnetic and resulting software have made it easier to analyze complex problems and design configurations. CST Microwave Studio is the powerful and easy-to-use electromagnetic field simulation software, based on Finite Integration Method. This is a fully featured software package for electromagnetic analysis and design in the high frequency range.

Simulation of input characteristics of RDRA in free space and in presence of phantom muscle layer and SAR distribution in the phantom muscle layer due to the antenna was carried out using CST Microwave Studio software. The input characteristics of the antenna include the variations of return loss and VSWR versus frequency and the values of input resistance at resonance with and without phantom muscle.

Various aspects involved in the process of simulation using CST Microwave Studio software are given below. The process of inputting the structure is easy and strong graphic feedback simplifies the definition of our device even further. After the component has been modeled, a fully automatic meshing procedure is applied before a simulation is started. This software fully based on method on demand approach allows using the simulator or mesh type that is best suited

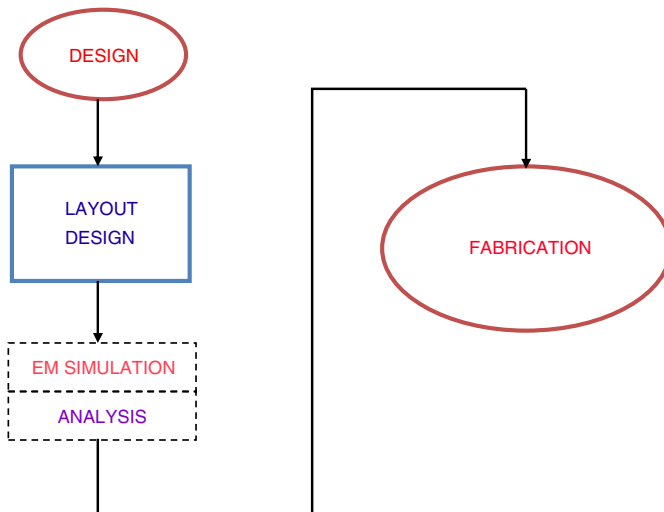
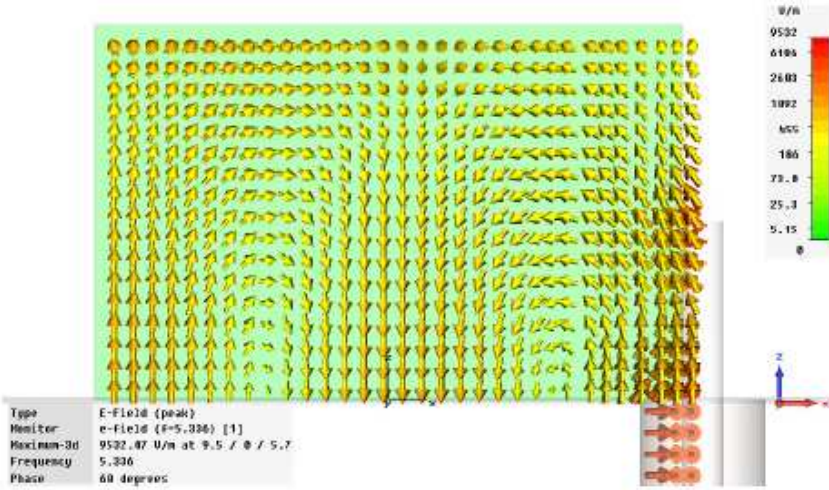
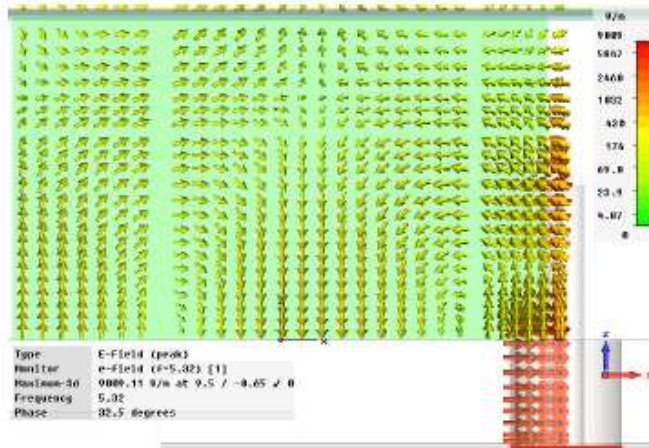


Figure 2. The design and simulation workflow.

to a particular problem which gives outstanding performance. CST Microwave Studio software is especially suited to the fast as well as efficient analysis and design of components like antennae (including arrays), filters, transmission lines, couplers, connectors (single and multiple pin), printed circuit boards, resonators and many more [14].



(a)



(b)

Figure 3. Electric field distribution in the RDRA. (a) In free space. (b) In the bio-medium.

The flow chart for the design, simulation and fabrication for dual segment RDRA is shown in Figure 2. In simulation, CST Microwave Studio software has been introduced for layout design and simulation. Analysis of simulation results has been made to get optimum results before proceeding to the fabrication process.

4. RESULTS AND DISCUSSION

4.1. Near Field Distribution

The simulation study of field distribution in the proposed RDRA has been carried out at 5.336 GHz, the simulated value of resonant frequency of antenna in free space (given in Section 4.2) using CST Microwave Studio software. When RDRA is excited using 50 Ω coaxial probe as shown in Figure 1, the electric field distributions shown in Figure 3 are obtained. It is apparent from Figure 2 that the coaxial probe excites $TE_{2\delta 1}^y$ higher order mode fields in the RDRA in free space. This higher order mode is excited within the RDRA because of the high aspect ratios with high surface to volume ratio [12]. The high aspect ratios with high surface-to-volume ratio of the RDRA provide wide bandwidth. The mode of operation and field distribution are disturbed when the bio-medium is placed in the vicinity of the antenna. The deviation in field distribution may be due to the reflections/scattering caused by abrupt changes in the media.

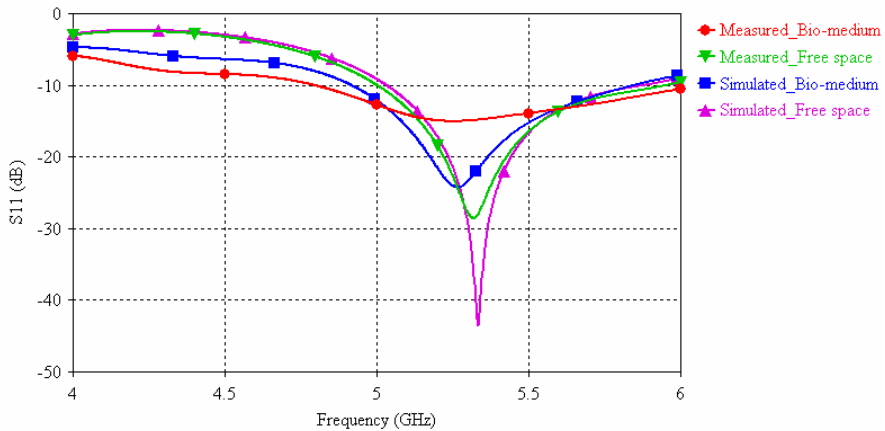


Figure 4. Return loss versus frequency characteristics of RDRA.

4.2. Return Loss and Input VSWR Versus Frequency Characteristics

The return loss and input VSWR of RDRA in free space and in presence of phantom muscle layer were measured at different frequencies over 4.0–6.0 GHz range using Agilent PNA series Vector Network Analyzer (Model No. E8364B) and these parameters were also obtained through simulation using CST Microwave Studio software. The measured and simulated variations of return loss and input VSWR as functions of frequency for the RDRA in free space and in the presence of phantom muscle layer when it is separated from the antenna by miler sheet of thickness equal to 0.2 mm are shown in Figures 4 and 5 respectively. From Figure 4 the resonant frequency and percentage bandwidth of the proposed RDRA in free space are extracted and the results are shown in Table 1. From Table 1, it can be observed that the measured resonant frequency of antenna in free space are nearly in agreement with theoretical and simulated values. The measured bandwidth of the antenna in free space is in agreement with the simulated value. The theoretical bandwidth of antenna in free space deviates from experimental/simulated values. The deviation in the results may be due to effect of finite ground plane not considered in theoretical computation. The experimental/simulated results show that the antenna provides wide bandwidth, which may be due to the high aspect ratio with high-surface-to-volume ratio of the RDRA.

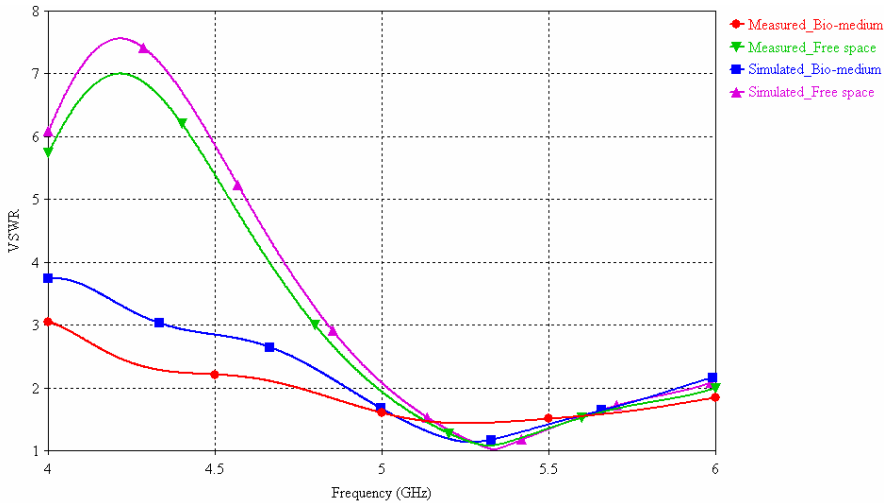


Figure 5. VSWR versus frequency characteristics of RDRA.

Table 1. Return loss parameters of RDRA.

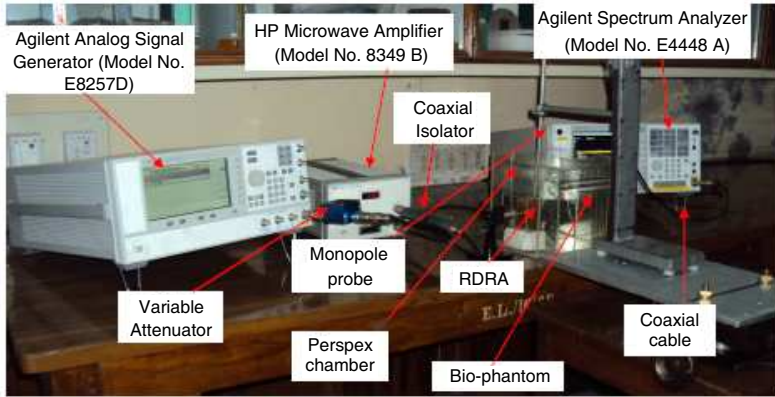
Parameters		Resonant Frequency	% Bandwidth
Theoretical (In Free Space)		5.227 GHz	7.405
Measured	In Free Space	5.32 GHz	17.63
	In Bio-medium	5.25 GHz	> 22.93
Simulated	In Free Space	5.336 GHz	15.54
	In Bio-medium	5.266 GHz	17.58

The simulated values of input resistance at resonance for RDRA in free space and in presence of phantom muscle layer are found to be $46.75\ \Omega$ and $46.55\ \Omega$ respectively. This may provide good impedance matching of the antenna with $50\ \Omega$ coaxial probe feed. The resonant frequency of the antenna in combination with coaxial probe is considered here in the estimation of input resistance.

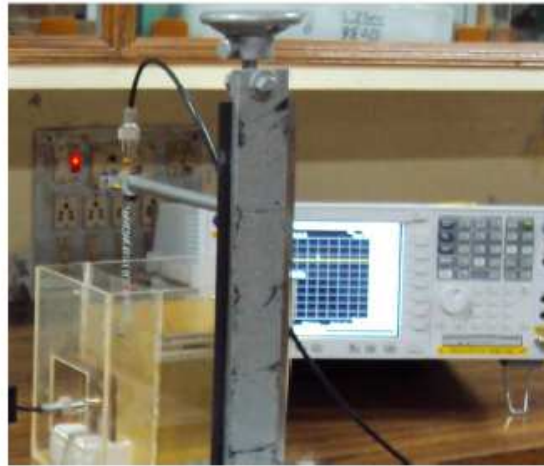
From Figures 4–5 and Table 1, it can be seen that measured resonant frequency of RDRA in presence of phantom muscle is 5.25 GHz, which is 70 MHz lower than the resonant frequency of antenna in free space. Also, the simulated resonant frequency in presence of phantom muscle is 5.266 GHz, which is 70 MHz lower than the resonant frequency of antenna in free space. The bandwidth of RDRA in the presence of phantom muscle is greater than the corresponding value in free space. The frequency de-tuning in presence of phantom muscle layer may be attributed to the perturbation in the resonator mode and near field distribution for $TE_{2\delta 1}^y$ mode as shown in Figure 3. The improvement in bandwidth of RDRA in presence of phantom muscle may be attributed to loading of the antenna with lossy medium. From Figures 4 and 5, it can be observed that the values of return loss and input VSWR of the RDRA in presence of phantom muscle are higher than the corresponding parameter values of antenna in free space. This may be attributed to wave reflections due to abrupt changes in the medium when antenna is in the vicinity of the bio-medium.

5. EXPERIMENTAL TECHNIQUE FOR MEASURING FIELD COMPONENTS IN PHANTOM MUSCLE LAYER

The experimental setup for measuring the power levels proportional to square of the magnitude of induced electric field components in artificial muscle medium separated from RDRA by miler sheet of thickness equal to 0.2 mm is shown in Figure 6. The measured power levels have been used to determine SAR distribution in the artificial



(a)



(b)

Figure 6. (a) Experimental setup for electric field intensity measurement. (b) Expanded view of a part of the setup including phantom muscle and coaxial monopole probe.

muscle at the measured resonant frequency of 5.25 GHz in the presence of phantom muscle layer.

Agilent make analog signal generator (Model No.: E8257D) was connected to the fabricated RDRA through a Narada make step attenuator (Model No.: 5745.69), HP 2–20 GHz microwave amplifier (Model No.: 8349 B, Max. 20 dBm power) and Microlab make coaxial isolator (Model No.: N157C). A coaxial monopole probe was connected

to RF-In port of Agilent Spectrum Analyzer (Model No. E4448 A, 3 Hz–50 GHz, –152 dBm Displayed Average Noise Level (DANL) for 3–6.6 GHz). When microwave power was fed to RDRA from the source and amplifier, a part of power was transmitted into artificial muscle, which was separated from the antenna by miler sheet of thickness equal to 0.2 mm. The power sensed by the monopole probe inserted at appropriate location in the artificial muscle is fed back to RF-In port of the spectrum analyzer. Two 50 Ω coaxial monopole probes (L-shaped and straight) procured from M/S. Vidyut Yantra Udyog, Modinagar, U.P., India were used in the measurement. The dimensions of the extended inner conductor of the L-shaped coaxial probe are: Length = 12.0 mm, and diameter = 1.0 mm. The length and diameter of the extended inner conductor of the straight coaxial are respectively equal to 14.0 mm, and 1.5 mm. The spectrum analyzer was configured to measure the power levels proportional to square of the magnitude of induced electric field components at different frequencies of interest. The experimental determination of SAR distributions in artificial muscle was done as detailed below. The power level corresponding to Z -component of induced electric field at a point in phantom muscle, which is proportional to $|E_z|^2$ was measured as a function of distance along X -/ Y -/ Z -directions by keeping the tip side of L-shaped monopole probe axis along Z -direction and moving it in the desired direction (X -, Y - or Z -direction) keeping other coordinates fixed. The power levels corresponding to X - and Y -components of induced electric field at a point in phantom muscle, which are proportional to $|E_x|^2$ and $|E_y|^2$ respectively were measured using straight probe by keeping its axis along X - and Y -directions respectively. These components as a function of distance along X -/ Y -/ Z -directions were obtained by moving the straight probe in the desired directions (X -, Y - or Z -direction) keeping other coordinates fixed. The differing responses of the L-shaped and straight probes in measuring same component at a frequency have been taken care of by using calibration factor. The square of the magnitude of total induced electric field $|E|^2$ at any position of phantom muscle is given by

$$|E|^2 = |E_x|^2 + |E_y|^2 + |E_z|^2 \quad (6)$$

where, E_x , E_y and E_z are the components of electric field along X , Y and Z directions respectively. The power levels proportional to square of the magnitude field values were sampled at a number of positions from 0 to ± 6 cm along each of the X - and Y -directions and from 0 to 6 cm along Z -direction for RDRA operating at the resonant frequency of 5.25 GHz. The measured power levels were converted to relative specific absorption rate (SAR) by utilizing Equation (5). The density of muscle was taken equal to be 1050 kg/m³ in computation [15].

The accuracy in the measurement of distance along X -/ Y -/ Z -directions is 1mm. The error in measurement of power levels (proportional to $|E_x|^2/|E_y|^2/|E_z|^2$) is ± 0.01 dB. Although the probe position could not be measured to the degree of accuracy required for precision measurements, it was sufficient to prove the feasibility of this technique.

6. RADIATION PATTERN

The simulated radiation patterns of the RDRA in free space as well as in the presence of phantom muscle at respective resonant frequencies are given in Figure 7. From Figure 7, it can be observed that the

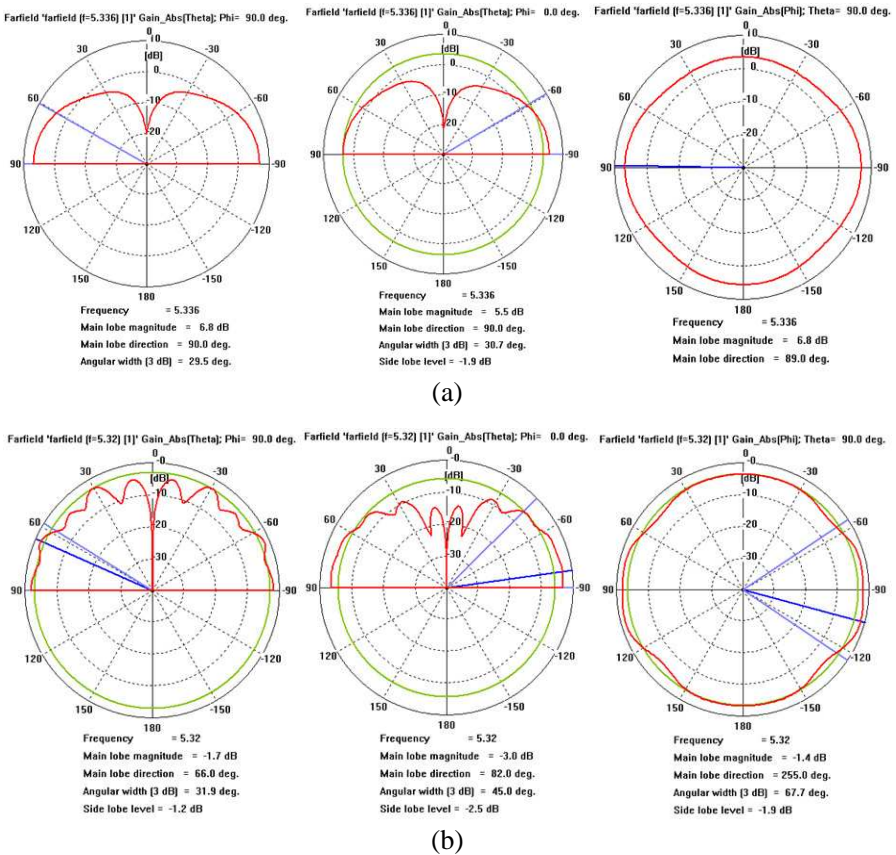


Figure 7. Radiation pattern of RDRA. (a) In free space. (b) In bio-medium.

RDRA in free space provides monopole type of radiation pattern and the presence of phantom muscle distorts the radiation patterns as compared to those in free space.

7. SAR DISTRIBUTION

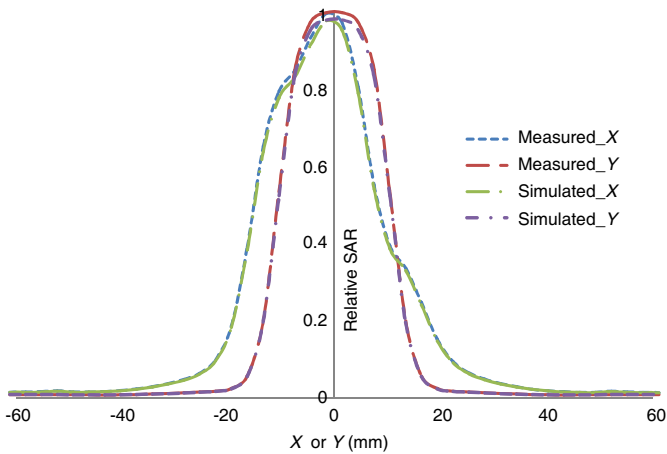
Within a given volume of body tissue the rate of energy absorption is proportional to the square of the magnitude of induced electric field strength. This parameter is called the specific absorption rate (SAR) and is expressed in W/kg [1]. SAR can be computed with the help of the standard relation given below,

$$\text{SAR} = \frac{\sigma |E|^2}{2\rho} \quad (7)$$

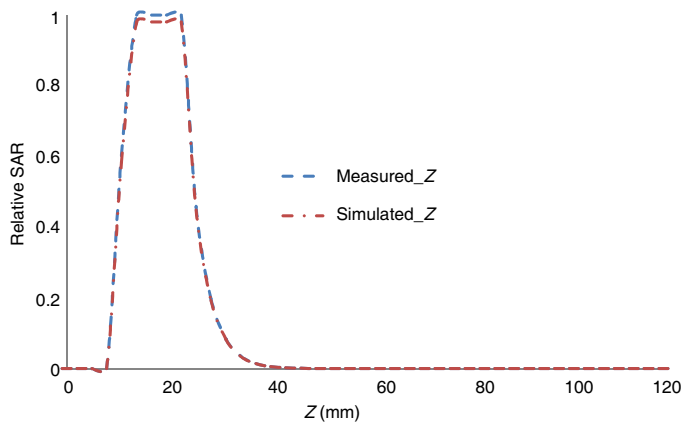
where $|E|$ is the magnitude of total electric field intensity in the bio-medium, σ and ρ are respectively the conductivity and density of the bio-medium.

The relative SAR distribution in phantom muscle medium in close proximity with the proposed RDRA at the measured resonant frequency of 5.25 GHz was determined through simulation as well as experimentally. The simulated SAR distribution in muscle layer was obtained using CST Microwave Studio software whereas experimental distribution was determined with the help of a coaxial monopole probe and Agilent Spectrum Analyzer (Model No. E4448A). The simulated and experimental SAR distributions in the phantom muscle due to RDRA are compared at the measured resonant frequency of 5.25 GHz (Figure 8). The simulated and corresponding experimental results for SAR distributions are close to each other.

From Figure 8, it can be observed that experimental SAR values are deviate somewhat from corresponding simulated values. This deviation may be due to the measured resonant frequency of 5.25 GHz not matching exactly with the simulated value and also because of error in measuring the position of the monopole probe which affects the accuracy of measured results. Interaction between the probe and the RDRA may also occur. Although, these factors could cause negligible effect on SAR-value independently but taken collectively may become significant and cause the mismatch between simulated and experimental SAR values. From Figure 8 it may be noted that measured SAR distribution in X -direction is wider than that in Y -direction. This may be due to the effects of near field distributions and spurious radiation from the coaxial probe used for excitation of antenna which is located on X -direction in the central region of right face of the RDRA in Y - Z plane.



(a)



(b)

Figure 8. Variation of relative SAR in muscle with distance along (a) X- or Y-direction, (b) Z-direction.

The two parameters of importance for obtaining the volume of the tissue absorbing significant amount of power are effective field size (EFS) and penetration depth. The EFS is defined as the area enclosed within the 50% SAR contour inside the tissue. The penetration depth is the depth at which SAR becomes $1/e^2$ of its value at the surface [15]. The SAR value in phantom muscle is normalized with respect to value at the antenna-muscle interface. The values of EFS and penetration depth are extracted from Figure 8. The simulated values of EFS and penetration depth in phantom muscle layer are

$23.62 \times 20.50 \text{ mm}^2$ and 18.5 mm respectively, while the measured values of EFS and penetration depth are $23.64 \times 20.50 \text{ mm}^2$ and 18.5 mm respectively. The simulated values of EFS and penetration depth in muscle layer are in agreement with measured values. Finally, it is noted that maximum simulated value of SAR (10 g) are found to be 6.87 W/kg at the point $(-0.66, -0.325, 22.9185)$ for input power of 0.2 W , which is above safe level ($= 2 \text{ W/kg}$) for public exposure as per ICNIRP recommendations. Though maximum simulated value of SAR is reported in the manuscript for input power of 0.2 W , the power level used in measurement is 19.5 dBm (89.12 mW). At the power level used in the measurement maximum simulated value of SAR is found to be 3.061 W/kg , which is still above safe level (2 W/kg) for public exposure as per ICNIRP recommendations.

8. CONCLUSION

The simulation and experimental studies of SAR distributions in a phantom muscle layer in close proximity with the RDRA fabricated from $(\text{CaO}.4\text{ZnO}. \text{Nb}_2\text{O}_5, \text{TiO}_2)$ ceramic material in C-band of microwave frequencies have been described. The simulated SAR distribution in muscle has been determined through CST Microwave Studio simulation software and measured distribution obtained using L-shaped and straight monopole probe and Agilent make spectrum analyzer. The measured results of resonant frequency of the RDRA in free space as well as SAR distributions in muscle layer are close to simulated and/or theoretical results. The experimental bandwidth of antenna in free space agrees well with the simulated value. But the theoretical bandwidth of antenna in free space deviates from experimental/simulated values. The deviation in the results may be due to effect of finite ground plane not considered in theoretical computation. It is inferred from experimental and simulation results that the antenna operates in wide bandwidth which may be due to the high aspect ratio with high-surface-to-volume ratio of the RDRA. The experimental SAR distributions deviate somewhat from corresponding simulation distributions. the deviation may be due to experimental resonant frequency in presence of phantom muscle not matching with the simulation value and also because of errors in measurement of probe position and power level. The results presented here may find potential application in wireless communication and telemedicine fields for designing a ceramic antenna and evaluating the power absorption in a bio-medium due to the antenna. The investigation on the antenna located close to phantom muscle for different antenna-to bio-medium separations may be taken up in future studies.

REFERENCES

1. Okoniewski, M. and M. A. Stuchly, "A study of the handset antenna and human body interaction," *IEEE Trans. on Microwave Theory and Techniques*, Vol. 44, No. 10, 1855–1864, 1996.
2. Lautru, P. D., M. F. Wong, V. H. Fouad, and J. Wiart, "Rigorous evolution of specific absorption rate (SAR) induced in a multilayer biological structure," *European Microwave Conference*, Vol. 3, 2005.
3. Mongia, R. K. and P. Bhartia, "DRA — A review and general design relation for resonant frequency and bandwidth," *International Journal of Microwave and Millimeter Wave Computer — Aided Engineering*, Vol. 4, No. 3, 230–247, 1994.
4. Ittipiboon, A. and R. K. Mongia, "Theoretical and experimental investigations on rectangular dielectric resonator antennas," *IEEE Transactions on Antennas and Propagation*, Vol. 45, No. 9, 1348–1356, Sep. 1997.
5. Rezaei, P., M. Hakkak, and K. Forooghi, "Design of wide-band dielectric resonator antenna with a two-segment structure," *Progress In Electromagnetics Research*, Vol. 66, 111–124, 2006.
6. Kajfez, D. and A. A. Kishk, "Dielectric resonator antenna-possible candidate for adaptive antenna arrays," *Proceedings VITEL 2002, International Symposium on Telecommunications, Next Generation Networks and Beyond*, Portoroz, Slovenia, May 13–14, 2002.
7. Saed, M. A. and R. Yadla, "Microstrip-FED low profile and compact dielectric resonator antennas," *Progress In Electromagnetics Research*, Vol. 56, 151–162, 2006.
8. Zainud-Deen, S. H., E. El-Deen, H. A. Sharshar, and M. A. Binyamin, "Design of UMTS dielectric resonator antenna for mobile phone including the biological effects," *Proc. URSI 24th National Radio Science Conference (NRSC 2007)*, Vol. 35, 1–8, Faculty of Engineering, Ain Shams Univ., Egypt, 2007.
9. Lee, T. H., R. A. Abd-Alhameed, and P. S. Excell, "New dielectric resonator antenna design for mobile handsets," URSI-2005, [http://rp.iszf.irk.ru/hawk/URSI2005/pdf/BP.10\(01068\).pdf](http://rp.iszf.irk.ru/hawk/URSI2005/pdf/BP.10(01068).pdf), 2005.
10. Palikruru, V. K., K. Sonoda, R. Surenran, and H. Jantunen, "BST-COC composite based rectangular dielectric resonator antenna (DRA) for 2.4 WLAN wrist applications," *Progress In Electromagnetics Research C*, Vol. 16, 195–205, 2010.

11. Petosa, A., *Dielectric Resonator Antennas Handbook*, 73–77, Artech House, Boston, London, 2007.
12. Rashidian, A. and D. M. Klymyshyn, “On the two segment and high aspect ratio rectangular dielectric resonator antenna for bandwidth enhancement and miniaturization,” *IEEE Transactions on Antennas and Propagation*, Vol. 57, No. 9, 2775–2780, Sep. 2009.
13. Zhou, J., D. Hara, and T. Kobayashi, “Development of ultra wideband electromagnetic phantoms for antennas and propagation studies,” *First European Conference on Antennas and Propagation (EuCAP 2006)*, 1–6, Nov. 6–10, 2006. doi: 10.1109/EUCAP.2006.4584884.
14. CST GmbH 2006 CST Microwave Studio (r) User Manual V.6.0, Darmstadt, Germany, www.cst.de, 2006.
15. Ebrahimi-Ganjeh, M. A. and A. R. Attari, “Study of water bolus effect on SAR penetration depth and effective field size for local hyperthermia,” *Progress In Electromagnetics Research B*, Vol. 4, 273–283, 2008.